

## HOTFIRE TESTING OF A SSME HPOTP WITH AN ANNULAR HYDROSTATIC BEARING

Steven A. Nolan and Robert I. Hibbs  
 Rockwell International  
 Rocketdyne Division  
 Canoga Park, California

and

Gary G. Genge  
 NASA George C. Marshall Space Flight Center  
 Marshall Space Flight Center, Alabama

E20-37  
 12864  
 P-21

### Abstract

A new fluid film bearing package has been tested in the Space Shuttle Main Engine (SSME) High Pressure Oxygen Turbopump (HPOTP). This fluid film element functions as both the pump end bearing and the preburner pump rear wear ring seal. Most importantly, it replaces a duplex ball bearing package which has been the primary life limiting component in the turbopump. The design and predicted performance of the turbopump are reviewed. Results are presented for measured pump and bearing performance during testing on the NASA Technology Test Bed (TTB) Engine located at Marshall Space Flight Center, Alabama. The most significant results were obtained from proximity probes located in the bearing bore which revealed large subsynchronous precession at ten percent of shaft speed during engine start which subsided prior to mainstage power levels and reappeared during engine shutdown at equivalent power levels below 65% of nominal. This phenomenon has been attributed to rotating stall in the diffuser. The proximity probes also revealed the location of the bearing in the bore for different operating speeds. Pump vibration characteristics were improved as compared to pumps tested with ball bearings. After seven starts and more than 700 seconds of testing, the pump showed no signs of performance degradation.

### Introduction

Annular seals were developed and used as leakage control devices and in that capacity were designed for optimum pump efficiency. Lomakin<sup>1</sup> pointed out that annular seals develop significant direct stiffness while in the centered, zero-eccentricity position and can influence the rotordynamics of a pump. Later, Black<sup>2</sup>, Jenssen<sup>3</sup>, and Black and Jenssen<sup>4,5</sup> investigated and explained the influence of seal forces on the rotordynamic behavior of pumps.

The term damper seal was conceived to describe an annular seal which has been intentionally roughened. This definition grew out of the work by von Pragenau<sup>6</sup> who analytically predicted that roughness in an annular seal would increase damping and reduce leakage. This was subsequently supported by the test data and analysis of Childs and Kim<sup>7,8,9</sup>, Childs and Garcia<sup>10</sup>, and Kim and Childs<sup>11</sup>. Childs tested many different roughness patterns including hole, post, sawtooth, knurl, helically grooved, and circumferentially grooved. The test results showed that rough seals

produced more damping than smooth seals and that the hole pattern seal could be optimized for maximum damping.

The first intentional implementation of damping seal technology was in the SSME Phase II HPOTP shown in Figure 1. Wear ring labyrinth seals on the Phase I preburner pump impeller were replaced with damping seals. The knurl pattern and process were developed at Rocketdyne specifically for this purpose and were subsequently tested by Childs and Kim<sup>7</sup>. Significant reductions in pump dynamic loads and improvement in rotor stability resulted.

During SSME testing, ball bearing wear has been a recurring life limiting issue. Primarily, the wear of the pump end bearings has limited the life of the turbopump and has necessitated periodic refurbishment. Recently, there have been several events during the testing of the SSME HPOTP which resulted in reduced ball bearing stiffness indicating that the turbopump could operate safely on the damping seal alone. A subsequent review of component measurement and test data from previous testing showed that the turbopump had operated safely on the damping seal alone a minimum of six different times without significant degradation in performance. Based on this evidence, redesign of the turbopump without pump end ball bearings seemed feasible.

The design concept chosen is illustrated in Figure 2 (Scharrer et al.<sup>12</sup>). The figure shows that the pump end bearings could be eliminated in favor of a single damping seal located at approximately the same axial plane. Since the damping seal will now be the primary load carrying element, it has been renamed an annular hydrostatic bearing. This paper presents the predicted and experimentally measured performance of the bearing design. In addition, the rotordynamic and hydrodynamic performance of the hydrostatic bearing supported turbopump will be compared with that of the current ball bearing supported pump.

### Requirements

The bearing design required substantial parametric evaluation before arriving at the current fully tapered, fully roughened annular hydrostatic bearing design. Parametric studies of geometry and configuration were considered to optimize the design in order to meet the hydrodynamic and rotordynamic requirements of the pump end bearing for the SSME HPOTP. Details of the design considerations are presented in Scharrer et al.<sup>12</sup>. The final design is similar to the current Phase II SSME HPOTP preburner pump damping seal and its well documented performance in flight configuration SSME pumps.

The design objective was to increase the rotordynamic critical speed and stability margins as shown in Figure 3 as well as address the remaining turbine end bearings loads. It was also of particular interest to ensure the implementation of the pump end hydrostatic bearing did not result in detrimental loads on the remaining rolling element bearings. Based on these requirements the pump end bearing targets were 175 MN/m (1.0 E6 lbf/in) direct stiffness and 61.2 KN-s/m (350 lbf-s/in) direct damping. The geometry and clearance tolerances were optimized to meet this requirement. The rotordynamic coefficients of the bearing as a function of shaft speed and eccentricity were provided for the rotordynamic analysis. The analyses included coefficients for minimum, nominal, and maximum conditions resulting from potential variability of tolerances and pump operating conditions. Stability of the bearing was consistently good throughout the speed parametric as evidenced by the whirl frequency ratio (WFR) being constant at 0.30. The WFR is a ratio of the destabilizing forces, cross-coupled stiffness, over the stabilizing forces, damping times synchronous speed.

The impact of the pump end hydrostatic bearing on the turbine end ball bearing loads was evaluated with transient non-linear rotordynamic analyses performed over the entire pump operating speed range. The results of these analyses for the nominal predicted hydrostatic bearing coefficients are shown in Figure 4. It is evident from this data that the dynamic loads are significantly reduced for pump speeds above 27,000 RPM, which is the primary operating range of this pump. These reductions in alternating loads are a result of the increased critical speed margins on the second mode as well as the additional damping derived from the optimized bearing configuration. Alternating load reductions in excess of 30% are predicted for FPL operation, 30,000 RPM, and nominal hydrostatic bearing coefficients.

An additional important consideration was the start transient and the potential for substantial wear. Several configurations were considered which attempted to provide for both hydrodynamic performance during the start transient and hydrostatic performance at Full Power Level (FPL). The configurations considered were straight, tapered, partially tapered, rough, and partially rough. Although the configurations studied, as discussed in Scharrer et al.<sup>12</sup>, did show some slight advantages to having a partially roughened or partially tapered configuration, the benefits were not substantial enough to justify the added complexity and cost.

In addition to the load impact issue, the transient analysis was utilized to predict rotor deflections for all pump operating conditions. The deflection at the hydrostatic bearing was identified as a control point for the design. Specifically, a 0.0254 mm (.001 in.) margin against rubbing, between the rotor and stator at the hydrostatic bearing location, was the guideline for all bearing design ranges. This guideline ensured adequate rub margins at all other axial locations along the rotor. The maximum deflection of the rotor, fixed and alternating deflections combined, was used to identify this margin as shown in the sample rotor orbit prediction of Figure 5.

#### TTB Test Facility

The Technology Test Bed (TTB) facility at the Marshall Space Flight Center (MSFC) was designated choice for testing the axially fed hydrostatic bearing. The facility was developed to serve as an accessible platform with capability for testing new technology in large liquid rocket engines. The test stand, formally used for the first stage of the Saturn V, was reactivated in 1988 as a SSME facility. With run tank capacities of 89,000 liters (23,500 gallons) of liquid oxygen (LOX) and 284,000 liters (75,000 gallons) of liquid hydrogen, the TTB facility can operate an SSME over 200 seconds per test depending on the desired thrust profile. TTB can operate the SSME from the engine's upper limit of 111% of rated power level (RPL) to 80% of RPL while independently controlling the engine LOX and fuel inlet pressures. The facility can vary the LOX and fuel engine inlet net positive suction pressures (NPSP) over the acceptable range for the SSME. The facility actually operates from 137.9 to 1,034.2 KPa (20 to 150 psi) ullage pressure for LOX and 55.2 to 344.7 Kpa (8 to 50 psi) ullage pressure for fuel. Because of its technology advancement role, the data collection system has 750 digital channels, 50 samples per second, and 216 analog channels to measure pressure, temperature, vibrations, speed, proximity, and more.

#### Pump/Engine Instrumentation

The SSME HPOTP is equipped with pump and turbine end radial accelerometers as well as external strain gages which are typically used for high frequency data evaluation. The pump tested at TTB had five accelerometers on both the pump end and turbine flanges as well as four strain gages on the pump housing between the pump and turbine. The housing strain gages which are typically used for bearing generated frequency detection on Phase II HPOTPs were included on

the hydrostatic configuration as an additional redundant point of comparison. In addition to the standard instrumentation, the hydrostatic bearing HPOTP contained seven internal strain gages. These gages are located near bearing support locations and intended for qualitative comparison to existing Phase II pump data.

Proximity probes were installed in the bearing in order to provide data for the determination of bearing liftoff/touchdown, rotor position in the bore, rotor orbit size the overall health of the bearing. For this particular pump build, Kaman proximity probes were chosen. Two pressure and temperature measurement taps were included directly upstream of the bearing inlet and downstream of the bearing exit to assess the bearings performance. Additionally, two pressure sensors were located in the cavity downstream of the bearing to anchor overall pump performance.

### Test Plan

Health monitoring of the entire turbopump was a major issue when the turbopump was tested at TTB. Not only was the operational rubbing of the hydrostatic bearing a concern, but since the rotor response was changed the turbine end bearing life was an issue. Therefore all available means were taken to ensure that both the hydrostatic pump end bearing and the turbine end duplex ball bearings were not degrading. In addition to all of the standard SSME HPOTP post test inspections (rotor break/run torque, and visual inspection of turbine section, main pump inducer, number three bearing, and the preburner pump inlet) two additional measurements were included. The normal shaft travel measurement used on a test stand was replaced with a more precise measurement for measuring turbine bearing wear called shaft micro-travel described by Genge<sup>13</sup> and currently used for all flight HPOTPs. To ensure safety, the micro-travel acceptance limit was set at the current flight limit. The second post test measurement added was a radial "micro-wiggle" test which determined the amount of wear in the hydrostatic bearing. The wear guideline imposed on this measurement was set as the maximum wear found on the test article which had been exposed to 60 start/stop cycles in a test rig simulator reported by Scharer et al.<sup>14</sup>

Acceptance criteria also was set on all data obtained during the hot fire testing which directly related to the operation of either the hydrostatic bearing or the turbine end ball bearings. This included a requirement that the proximity probes show that the rotor lifts off the hydrostatic bearing surface prior to 1.51 seconds into the test, and that they show the rotor maintains a .0254 mm (.001 in.) radial clearance from the wall during operation. Limits were also placed on the minimum pressure drop across the hydrostatic bearing that would analytically show rotor stability, the temperature rise across the bearing that would indicate operational rubbing, and the pressures in the upstream or downstream cavities being greater than the structural analysis. The fluid exiting the hydrostatic bearing was also required to be a liquid, not two phase or gaseous. In addition, all of the standard SSME data limits were maintained for the testing of this turbopump. The TTB facility Optical Plume Anomaly Detector (OPAD) (Cooper et al.<sup>15</sup>) data was reviewed with a special emphasis on the presence of silver in the plume.

Initially, a four test series was planned which would characterize the performance of the hydrostatic bearing at all points in a test matrix containing four power levels and three LOX engine inlet NPSP values. During the test series, uncertainty with the proximity probes led to the addition of an additional test. The profiles and the test matrix which shows which test will evaluate that matrix condition are shown in Figures 6 through 11.

The primary objective of the first test was to demonstrate that the bearing had the capacity to lift off. However, due to thrust balance concerns with the HPOTP with tests between 1.5 seconds and

10 seconds, the test was planned for 10 seconds (Figure 6). With the complete 10 seconds, the immediate comparison of the predictions for 100% power level operations to results from the test also became an objective. The subsequent tests planned in the series were intended to assess the bearings capability at all power levels and engine inlet pressures available at TTB with bearing evaluation between each test.

Test two was intended to exercise all power levels without variations in inlet pressures to isolate any response due only to power level changes. With the confidence gained from the second test, the third test was meant to obtain as many of the combination of power level/LOX inlet pressure extremes as possible (Figure 8). From Figure 11, it can be seen that seven of the desired steady state conditions could be achieved. Once again, this test isolated all power level changes from LOX inlet pressure changes to allow the cause of any potential anomaly to be more easily understood. The fourth test profile was driven by four different factors. The main goals were to complete data collection for the test matrix and to start the pump with the lowest viscosity LOX allowed by the SSME Interface Control Document (or closest attainable by TTB). The low viscosity "hot LOX" would test the lift capability of the bearing in the worst possible fluid state that the bearing could undergo. Additionally a constant power level was maintained at the beginning of the test to evaluate proximity probe thermal characteristics. After completion of the fourth test, a fifth test was added to allow for the thermal stabilization of the proximity probes at all major power levels (Figure 10).

#### Test Run Summary

Testing began in March, 1992, with test TTB-029. In spite of a premature cut at 5.2 sec due to the High Pressure Fuel Turbopump (HPFTP) exceeding its turbine discharge temperature redline, examination of the test data showed the primary objective was achieved. Although the engine did not reach a steady state condition at 100% power level, rotor liftoff evaluation was possible. Additionally, this test did show an unexpected shaft orbit at low power levels which was determined to be caused by the rotating stall in the preburner pump impeller discussed later.

Because the primary objective had been achieved, it was decided to continue the series as originally planned. However the TTB-030 was also cut off prematurely only .32 seconds into the test. An engine oxidizer actuator position measurement showed that the valve was opening slower than is allowed during a normal start. Although the engine controller took action to correct the slow opening and was recovering, and the engine shut down as programmed.

With no objectives achieved in TTB-030, the next test profile was a repeat. The test went the full 85 second duration following the profile in Figure 7. All of the steady state data for the nominal engine inlet pressure were collected, and rotor stability was maintained throughout the 80% to 109% power level range. The next test followed the profile in Figure 8, and also went for its planned duration. This 205 second test acquired data at all but one of the remaining steady state operating points of interest. TTB-033 was initially meant to finish the series, but it was stopped prematurely due to a fire external to the engine not related to the pump. Post test inspections revealed a broken line had leaked hot gas. Repairs were performed, and TTB-034 ran the full 205 second duration as shown in Figure 9. This test successfully attained the 80% power level 827.4 KPa (120 psi) NPSP engine inlet condition, and warmer lox was used for the start transient without a change in performance. The final test in the series was performed in June, 1992. Unfortunately, the proximity probe output became highly erratic before the probes became thermally stable probe evaluation was not attained. This new design had performed well for a total of seven starts and 724.5 seconds.

### Bearing Performance

Bearing performance data analysis of the hydrostatic bearing on the TTB consisted of a determination of the performance of the bearing which included a repeatability evaluation, centered coefficient calculation, and an estimate of the dynamic load on the bearing. The repeatability evaluation showed no appreciable difference in the pressures and temperatures across the bearing, or the speed for 80%, 100%, 104%, and 109% power levels. This lack of discrepancy in the operational characteristics led to the small band between the maximum and minimum rotordynamic coefficients across the bearing. Based on orbit plots, the dynamic load on the bearing was estimated to be between 490 to 2050 N (110 to 460 lbf) for the tests at power levels between 80% and 109%. Data show that the bearing operated without any anomaly and could withstand the load experienced at the bearing location. The hydrostatic bearing could be run indefinitely without any problems provided that the operational characteristics remain within the trends of the data that has been collected to date.

Data was collected to determine the repeatability in the operational characteristics of the hydrostatic bearing from test to test. If the bearing pressures and temperatures remain unchanged from test to test at different operating speeds, the bearing performance is judged to be essentially unchanged. Typical data from the upstream and downstream pressures and temperatures are summarized in Table I. The data reviewed indicate only the downstream pressure indicate appreciable variance from test to test. Downstream pressures were approximately 345 KPa (50 psi) lower during low NPSH testing. However, because this difference is only a fraction of the total pressure drop, the performance of the bearing was essentially unchanged. Resulting pressures were below the vapor pressure of liquid oxygen but in order to vaporize the fluid must be at that state longer than the fluid is in the bearing. The velocity of the fluid at that point is approximately 400 m/s (1300 ft/s) for about .025 m (0.1 in.) which is approximately 6 microseconds. Under these conditions, the fluid could be approximately 690 KPa (100 psi) below the vapor pressure without cavitation.

Since the bearing did not experience substantial deviation in its operational characteristics, the band between the maximum and minimum empirical rotordynamic coefficients of the bearing was small. Figures 12 contains the values for direct stiffness, cross-coupled stiffness, and the direct damping of the bearing during the testing. These coefficients, owing to the fact that the operating conditions were in the range of the design, compared well with the coefficients predicted during the design phase. Load capacity versus eccentricity of the bearing is depicted in Figure 13 at each of the power levels. The coefficients showed only small differences in the maximum and minimum values verify the robustness of the hydrodynamic and bearing design. Although error in the actual values of the coefficients could be as high as 50 %, the coefficients generally were predicted in such a manner to provide a conservative design.

### Dynamic Data

The most significant dynamic data obtained from the hydrostatic bearing pump was provided by the proximity probes monitoring the rotor position at the hydrostatic bearing. No data observing actual rotor motion in the SSME HPOTP has previously been available. The major source of uncertainty relative to the proximity probe data was the probes calibration sensitivity to temperature changes. Due to the large thermal changes present when going from an ambient environment to a liquid oxygen environment absolute values of rotor position were difficult to determine. The most obvious indication of the probes temperature dependence is in the initial

"overshoot" seen in the proximity probe data, shown in Figure 14, after the pump reaches mainstage speed at approximately 4.2 sec. While some of the overshoot is due to pump thermal stabilization effects on the rotordynamic boundary conditions, a significant portion is due to the large temperature change experienced by the probe, approximately 40° R, during the start transient.

The proximity probe data obtained from this pump provided several interesting new insights into the operation of the SSME HPOTP, in addition to providing data that was directly comparable to the rotordynamic analytical predictions. The most readily identifiable phenomenon observed in the proximity probe data was a relatively low frequency large precession of the rotor during the start and cutoff transients. The precession is depicted in orbit plot of test TTB-029 in Figure 15 and clearly visible in the frequency domain data of Figure 16. Originally, this motion was thought to be synchronous shaft motion and that either the hydrostatic bearing stiffness was much less than predicted or the loads were much greater. However, further analysis showed that this motion actually occurs at 10% of synchronous speed during the start transient and did not track speed well during the shutdown transient. The precession started shortly after the initial pump rotations and dropped out at approximately 20,000 RPM. The amplitude remained relatively constant at a level between 0.12 and 0.14 mm (.005 and .006 in.) An investigation into possible excitation sources for this phenomena led to rotating stall in either the preburner or main pump.

The identification of rotor motion associated with the rotating stall was considered a significant revelation. This phenomena had been measured in the laboratory in water for both the main pump and preburner pump. However, the magnitude and duration of the resulting forces were never fully understood or appreciated. The pump speed for the measured stall limit for both the preburner and main pumps correspond to the speed at which the large motion ceased during start-up.

The discovery of this phenomenon in the rotor motion has been attributed to the fact that the proximity probe data was the first good data defining rotor orbit motion. As mentioned previously, the significance of the presence of the phenomenon in the hydrostatic bearing configuration led to a greater appreciation of its existence. Previous isolator strain gage data was only viewed from a bearing load standpoint with frequency content during the transient being difficult to observe. The characteristics associated with rotor motion during stall were quite consistent from test to test. A tabulation of several characteristics associated with the precession for all the tests are listed in Table II.

A comparison of data, obtained from Phase II pump isolator strain gage data and the hydrostatic bearing proximity probes, exhibiting this phenomenon is shown in Figures 17 and 18. Figure 17 is a comparison of the time history data during the start transient which clearly shows the same characteristics for both sets of data. Figure 18 contains an estimate of the dynamic loads calculated from both sets of data. The isolator strain gage loads were calculated with standard load reduction technique developed for these gages, while the hydrostatic bearing loads were estimated from the displacement and predicted bearing stiffness. It is evident that the loads are comparable and the deflections present are not unique to the hydrostatic bearing configuration.

Another interesting phenomenon discovered in the proximity probe data was that the rotor appeared to "center" itself in the bearing when the propellants filled the pump while the engine was being prepared for test. This occurred due to propellant pressure forces lifting the rotating assembly, which is almost vertical while attached to the engine, and bottoming the rotor on an axial stop which is perpendicular to the pump centerline resulting in the "straightening" the rotor assembly in the pump. The most attractive feature of this phenomenon was that although the shaft may not have been exactly "centered", it did not contact the journal when pump rotation began.

With no contact present there was no indication of liftoff during the start transient. This is significant since it indicates the rotor runs on a fluid film during the start transient and removes the opportunity for wear during engine start. Additionally, there appeared to be little indication of contact during the shutdown transient. No obvious indication of contact appears in the proximity probe data until at least 10 sec. after engine shutdown at which time the pump speed had dropped to very low levels. These rub characteristics appeared to be relatively benign in all tests. The time history data from a typical rub indication where the rotor deflections reach a limit or flat spot is shown in Figure 19. Indications of rub characteristics during the shutdown transients are tabulated in Table III.

While not as spectacular, the proximity probes also provided excellent data of rotor orbits and synchronous amplitudes during mainstage operation. Although, as previously mentioned, temperature dependant probe calibrations made it difficult to determine with great accuracy the absolute position of the rotor, the dynamic amplitudes, which are a much smaller portion of full scale, were more easily assessed for rotor orbit size. The significant conclusion with respect to this data is that the rotor orbits are very well behaved and comparable in magnitude for all mainstage power levels.

Synchronous RMS amplitude time histories from the proximity probe data over a test with significant power level and inlet conditions variations contain little variation in rotor orbit amplitude. An example of the RMS amplitude throughout a test which included operation at 80% RPL as well as 109% RPL with minimum inlet pressure, worst case conditions, is provided in Figure 20. The amplitudes presented in this example include the maximum and minimum values observed during all tests. Based on this data, the synchronous amplitudes of the rotating assembly were between 2.5 and 7 mV RMS, which corresponds to a peak to peak amplitude of between 0.005 and 0.015 mm (0.0002 and 0.0006 in.). Due to these small amplitudes, the potential error in the absolute value of the orbit size, due to calibration uncertainties, is believed to be less than .002 mm (0.0001 in.). Additionally, no significant harmonics of synchronous, other than those caused by blade wake forces as would be expected, were present in the data.

Although the absolute rotor position was difficult to discern due to probe calibration uncertainties, a fairly simple method was used in an attempt to anchor the rotor position with respect to the bearing bore. The alternative method used rotor orbits believed to be indicative of rub during shutdown as a means of locating the bearing bore and subsequently obtaining rotor positions relative to that point. It is believed that this method produced absolute rotor orbit positions representative of values for comparison to the analytical predictions. Using the data in this manner rotor orbit positions at various power level and vent conditions were predicted. A typical set of these results for test TTB-032 are shown in Figure 21.

The rotor positions and orbit amplitudes obtained from the proximity probe data compared favorably with orbit predictions from the rotordynamic analysis. To maintain the rub margins desired, the rotordynamic analyses predicted the fixed displacement at the hydrostatic bearing would be less than approximately 0.10 mm (0.004 in.) with peak to peak synchronous amplitudes in the range of approximately .025 mm (0.001 in.). Based on the results similar to those presented in Figure 21, the fixed displacements were between .051 and .10 mm (.002 and .004 in.) with the synchronous amplitudes somewhat less than 0.025 mm (.001 in.).

The data obtained from the standard external accelerometers and strain gages was evaluated on the same level as a typical Phase II HPOTP hotfire test for comparative purposes. The review consists of frequency domain data as well as time history data. All the data reviewed compared

favorably with a typical pump. The frequency domain data contained no significant anomalies or indications of detrimental conditions occurring during testing. Very slight indications of the low frequency precession phenomenon, which is atypical of external instrumentation, were present in the data. Harmonics of synchronous present in the data are comparable to those seen in the Phase II configuration.

The time history data for all instrumentation reviewed was nominal. Synchronous amplitudes were below 2 Grms on all accelerometers and below nominal Phase II pump values on a majority of the accelerometers. No significant amplitude changes were identified during power level excursions or inlet condition excursions. Additionally, composite RMS values and synchronous harmonic values were well within the Phase II database. A typical RMS amplitude time history of the synchronous amplitude from the accelerometer data is presented in Figure 22.

The turbine cartridge strain gages which, primarily intended for axial displacement measurements, were also reviewed for high frequency characteristics. Although low amplitude intermittent bearing cage harmonics were identified on these strain gages, this activity at a low amplitude is considered typical for this instrumentation which is so closely coupled with the bearing carrier, and is not considered to be detrimental. Additionally, the synchronous amplitudes were comparable to previously measured data from SSME pumps. The significance of this data is the confirmation that the implementation of the hydrostatic bearing did not result in any detrimental conditions at the turbine end bearings. This is of interest because the turbine bearing package contained separate modifications which have been demonstrated in other development pumps to resolve turbine bearing wear issues occasionally present in Phase II HPOTPS.

#### Plume Spectroscopy Information

The Optical Plume Anomaly Detector (OPAD) showed no conclusive evidence of silver during any test in this series. However, the OPAD system had not been calibrated for silver by plume seeding, and the NASA SP-273 chemical equilibrium code did not contain a complete set of reactants data for silver. Therefore, the system was limited to using primarily statistical methods with comparison to data collected on TTB tests 20 through 28, which had standard HPOTP bearing configurations. Because of this difficulty and the micro-wiggle measurements minimal silver, if any, was believed to have been ingested by the main injector.

#### Conclusions

The implementation of the hydrostatic bearing met or exceeded the rotordynamic requirements set forth. The data indicated no significant wear occurred due to rubbing during the transients and the rotor displacements were well behaved during all operating conditions. No rotordynamic issues resulted during the testing to 109% rated power levels and minimum NPSH, and the test program provided new insight into the operation of the SSME HPOTP.

#### References

<sup>1</sup>Lomakin, A., "Calculation of Critical Speed and Securing of Dynamic Stability of the Rotor of Hydraulic High Pressure Machines with Reference to Forces Arising in the Seal Gaps," *Energomashinostroenie*, Vol. 4, No. 4, pp. 1-5, April 1958.

<sup>2</sup>Black, H.F., "Effects of Hydraulic Forces in Annular Pressure Seals on the Vibration of Centrifugal Pump Rotors," Journal of Mechanical Engineering Science, Vol. 11, No. 2, pp. 206-213, 1969.

<sup>3</sup>Jensen, D.N., "Dynamics of Rotor Systems Embodying High Pressure Ring Seals," Phd.Dissertation, Heriot-Watt University, Edinburgh, Scotland, July 1970.

<sup>4</sup>Black, H.F. and Jenssen, D.N., "Dynamic Hybrid Properties of Annular Pressure Seals," Proc. Journal of Mechanical Engineering, Vol. 184, pp.92-100, 1970.

<sup>5</sup>Black, H.F. and Jenssen, D.N., "Effects of High Pressure Ring Seals on Pump Rotor Vibrations." ASME paper No. 71-WA/FE-38, 1971.

<sup>6</sup>von Pragenau, G., "Damping Seals for Turbomachinery,\* NASA TP-1987, March 1982.

<sup>7</sup>Childs, D.W. and Kim, C.-H., "Analysis and Testing for Rotordynamic Coefficients of Turbulent Annular Seals with Directionally Homogeneous Surface-Roughness Treatment for Rotor and Stator Elements," Trans. ASME Journal of Tribology, Vol. 107, July 1985, pp. 296-306.

<sup>8</sup>Childs, D.W. and Kim, C.-H., "Testing for Rotordynamic Coefficients and Leakage: Circumferentially-Grooved Turbulent Annular Seals," proceeding of the IFTOMM International Conference on Rotordynamics, Tokyo, Japan, Sept. 1986, pp. 609-618.

<sup>9</sup>Childs, D., and Kim, Chang-Ho, "Test Results for Round-Hole Pattern Damper Seals: Optimum Configurations and Dimensions for Maximum Net Damping, ASME Transactions, Journal of Tribology, Vol. 108, October 1986, pp. 605-611.

<sup>10</sup>Childs, D.W. and Garcia, F., "Test Results for Sawtooth Pattern Damper Seals: Leakage and Rotordynamic Coefficients," ASME Journal of Tribology, Vol. 109, January 1987, pp. 124-128.

<sup>11</sup>Kim, C-H, and Childs, D., "Analysis for Rotordynamic Coefficients of Helically-Grooved Turbulent Annular Seals," ASME Transaction Journal of Tribology, Vol. 109, January 1987, pp. 136-143.

<sup>12</sup>Scharrer, J.K., Hibbs, R.I., Nolan, S.A., and Nolan, S.A., "Extending the Life of the SSME HPOTP Through the Use of Annular Hydrostatic Bearings", AIAA paper no. 92-3401, July 1992.

<sup>13</sup>Genge, Gary G., "Developing Acceptance Limits for Measured Bearing Wear of the Space Shuttle Main Engine High Pressure Oxidizer Turbopump". AIAA 91-2412, 27th Annual Joint Propulsion Conference, June 24 to 26, 1991.

<sup>14</sup>Scharrer, J.K., Tellier, J.G. and Hibbs, R.I., "Start Transient Testing of an Annular Hydrostatic Bearing in Liquid Oxygen". AIAA 92-3404, 28th Annual Joint Propulsion Conference, July 6 to 8, 1992.

<sup>15</sup>Cooper, A.E., Powers, W.T., and Wallace, T.L. "OPAD Status Report: Investigation of SSME Component Erosion". SAE 921030, 1992 Society of Automotive Engineers Aerospace Atlantic Conference in Dayton, Ohio, April 7 to 10.

Table I: TTB Engine 4404 LOX Bearing Tests.

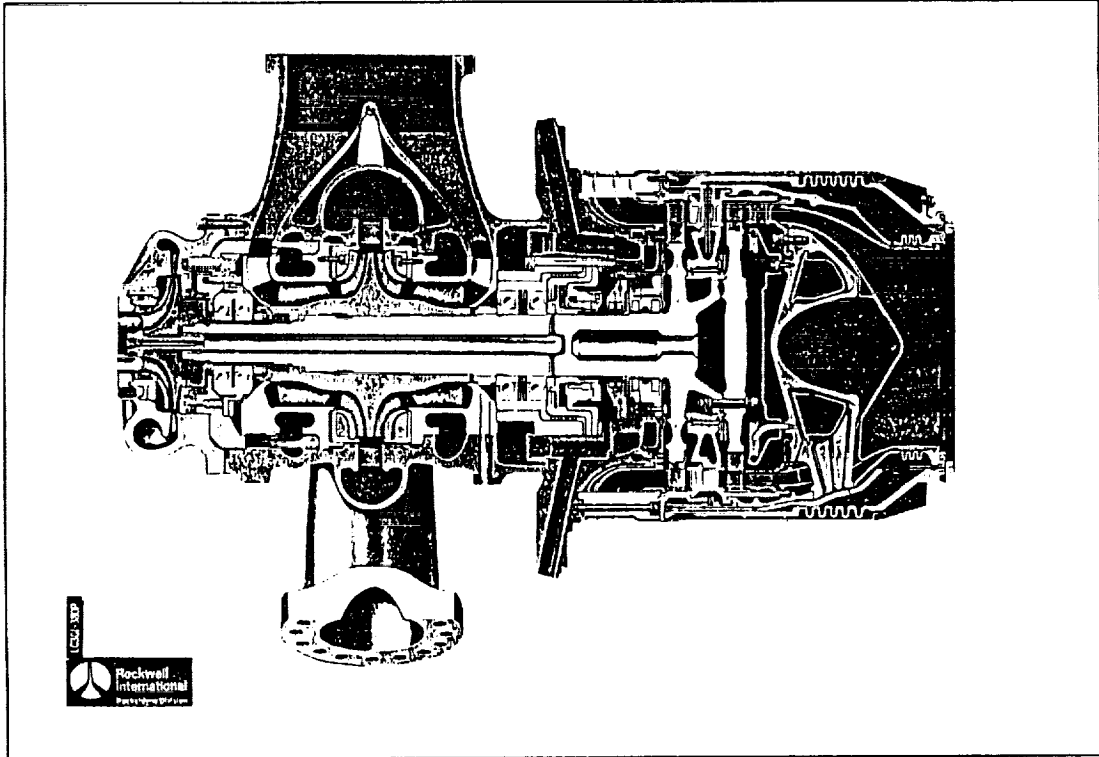
Power Level	Speed (rpm)	U/S Pr (psia)	D/S Pr (psia)	U/S Temp (R)	D/S Temp (R)
80	23,400	4150	210	199	212
100	27,700	5450	230	212	230
104	28,500	5700	250	216	233
109	29,700	6100	250	220	237

Table II: Precession Characteristics

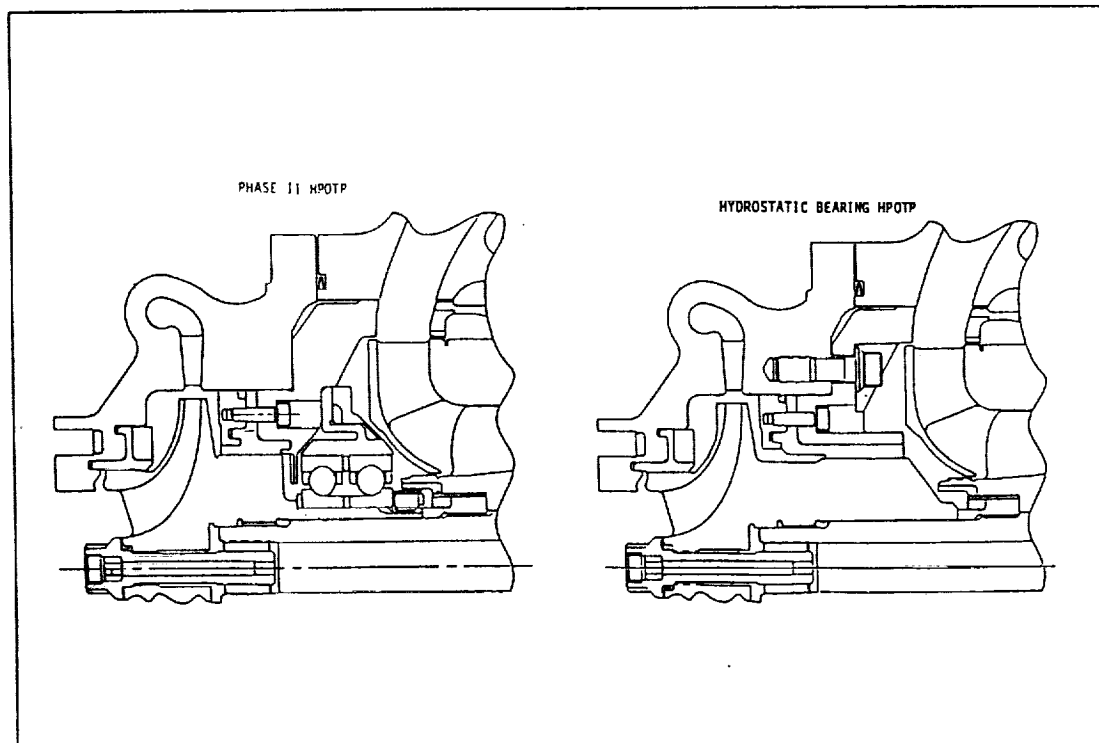
	Start Dropout		Cutoff Resumption	
	Time	Speed	Time	Speed
Test	E/S+sec	RPM	C/O+sec	RPM
801-029	3.05	20,400	0.5	16,800
801-030	N/A			
801-031	3.1	21,500	0.4	16,500
801-032	3.1	21,000	0.25	17,500
801-033	3.1	21,000	0.5	18,000
801-034	3.05	21,500	0.3	16,800
801-035	2.952	20,500	0.5	18,000

Table III: Rub Indications

	Time of Rub	Speed @Rub
Test	C/O+sec	RPM
TTB-029	11.0	550
TTB-030	None Obvious	
TTB-031	10.7	750
TTB-032	15.2	700
TTB-033	15.0	650
TTB-034	None Obvious	
TTB-035	14.0	700



**Figure 1.** Phase II SSME HPOTP.



**Figure 2.** Hydrostatic Bearing Modification.

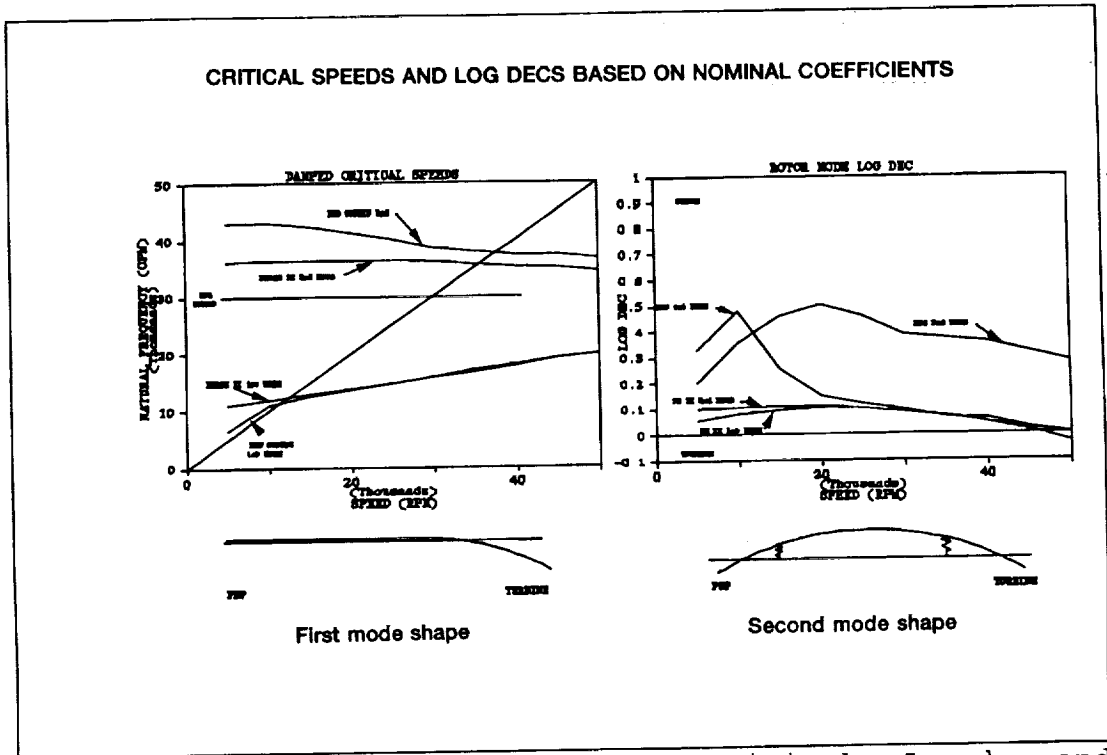


Figure 3. Rotordynamic Analysis- Critical Speeds and Stability.

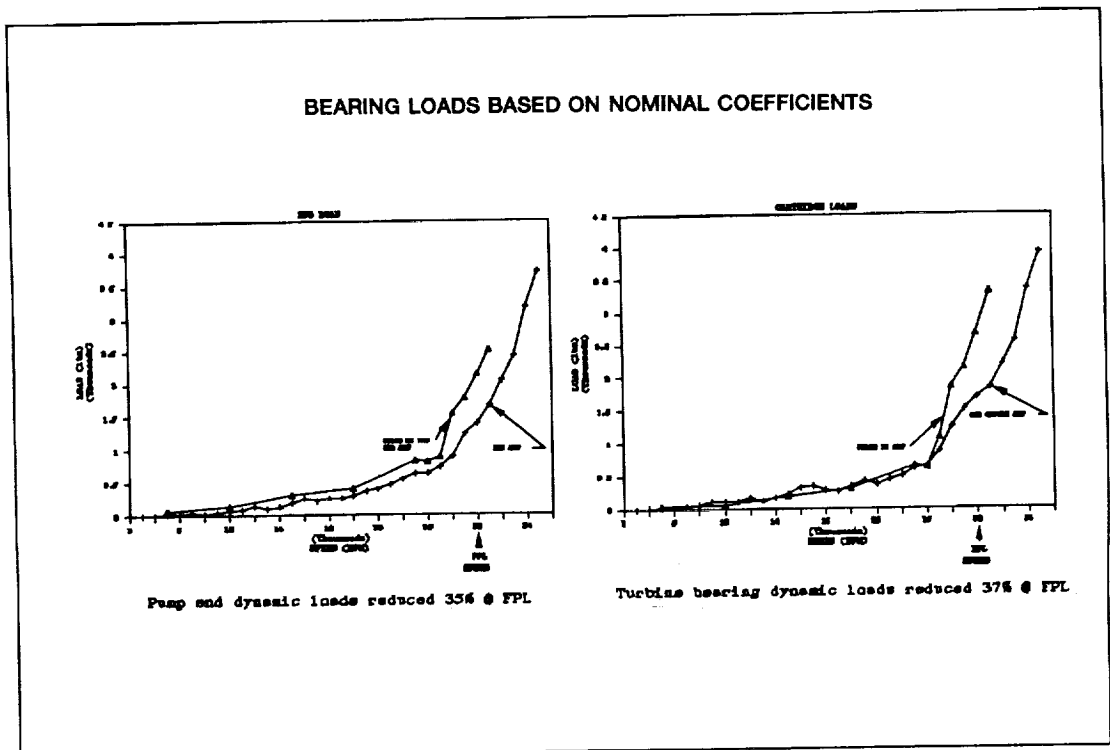


Figure 4. Bearing loads based on nominal coefficients.

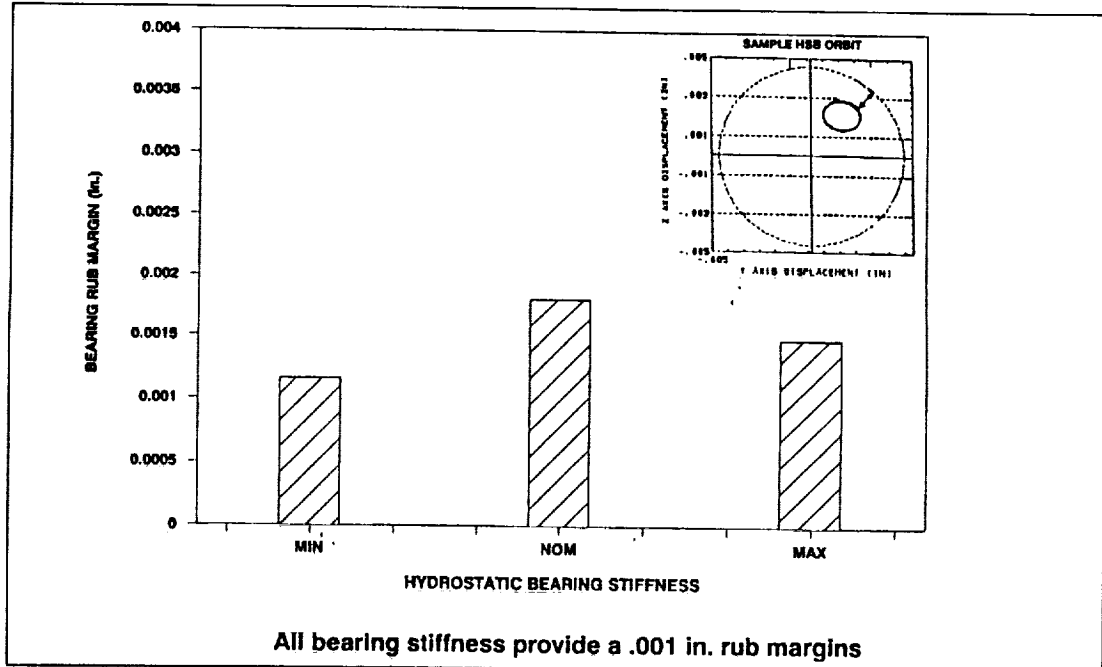


Figure 5. Maximum rotor orbit to minimum seal clearance margins.

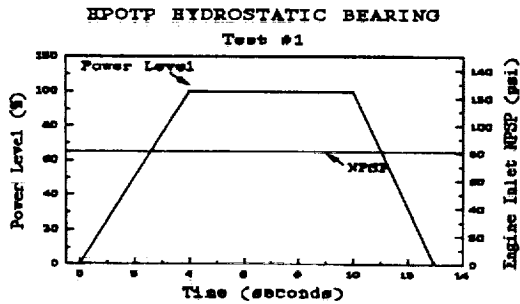


Figure 6. Hydrostatic bearing test #1.

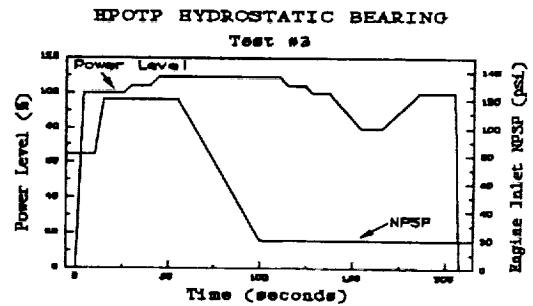


Figure 8. Hydrostatic bearing test #3.

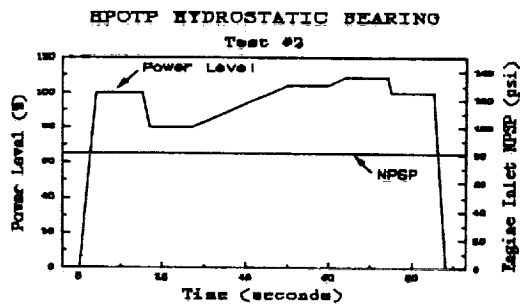


Figure 7. Hydrostatic bearing test #2.

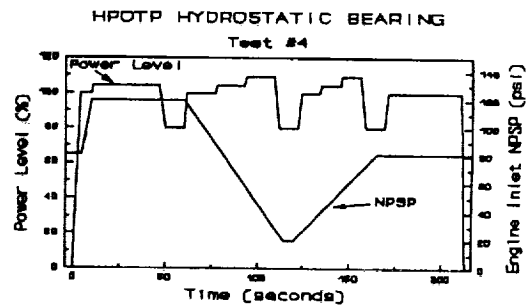


Figure 9. Hydrostatic bearing test #4.

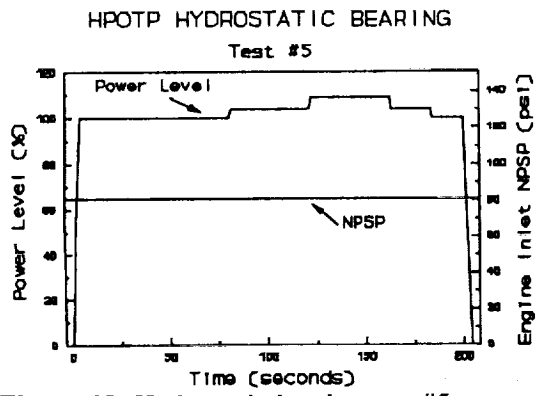


Figure 10. Hydrostatic bearing test #5.

		Engine Inlet NPSP (psi)		
		20	81	120
Power Level (%)	80	#3	#2	#4
	100	#3	#2	#3
	104	#3	#2	#3
	108	#3	#2	#3

Figure 11. Test condition matrix.

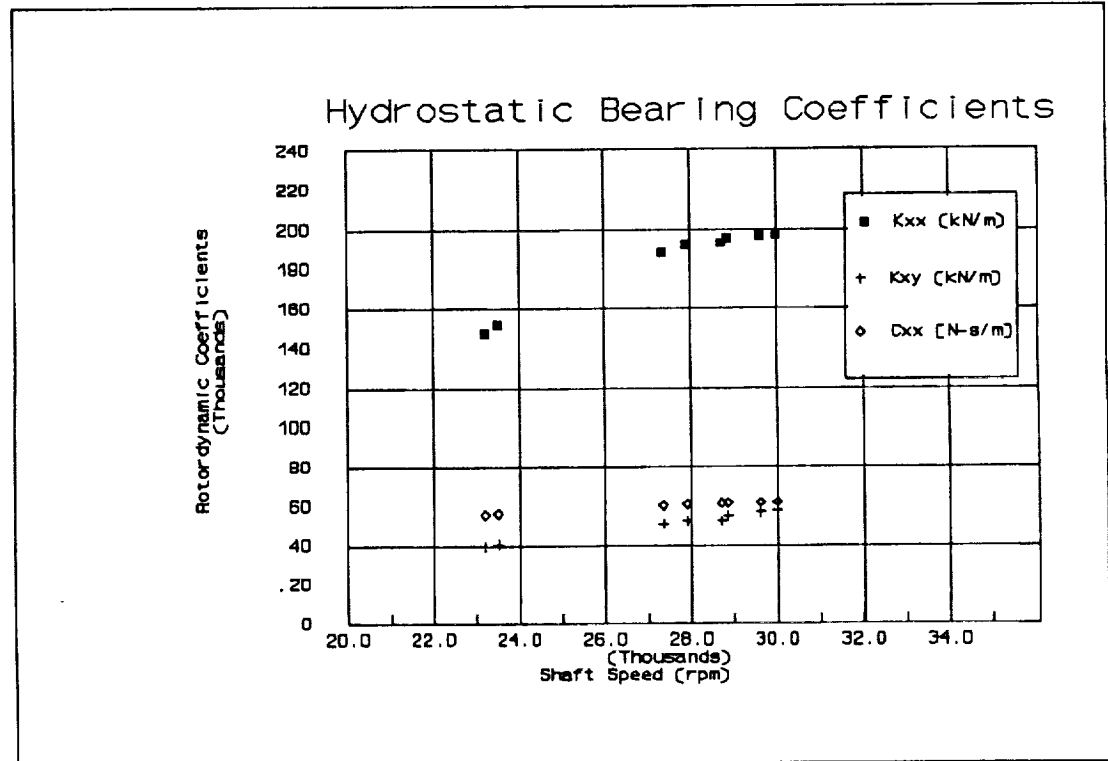


Figure 12. Hydrostatic bearing rotordynamic coefficients.

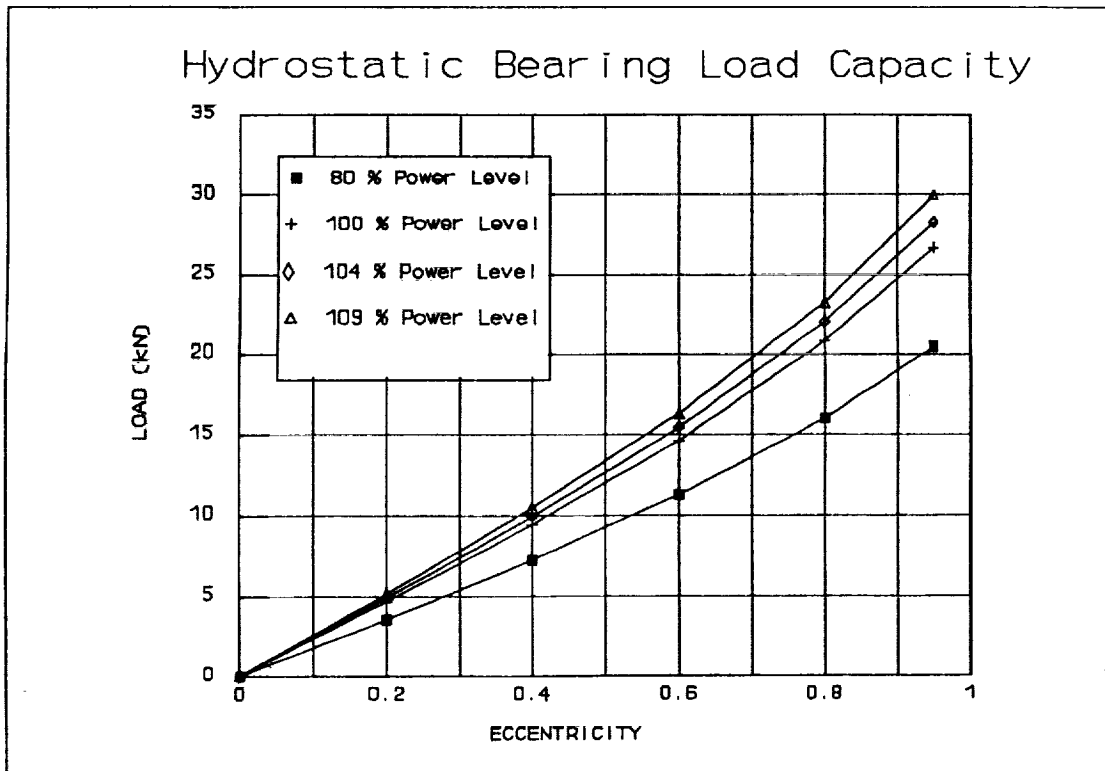


Figure 13. Hydrostatic bearing load capacity vs. eccentricity.

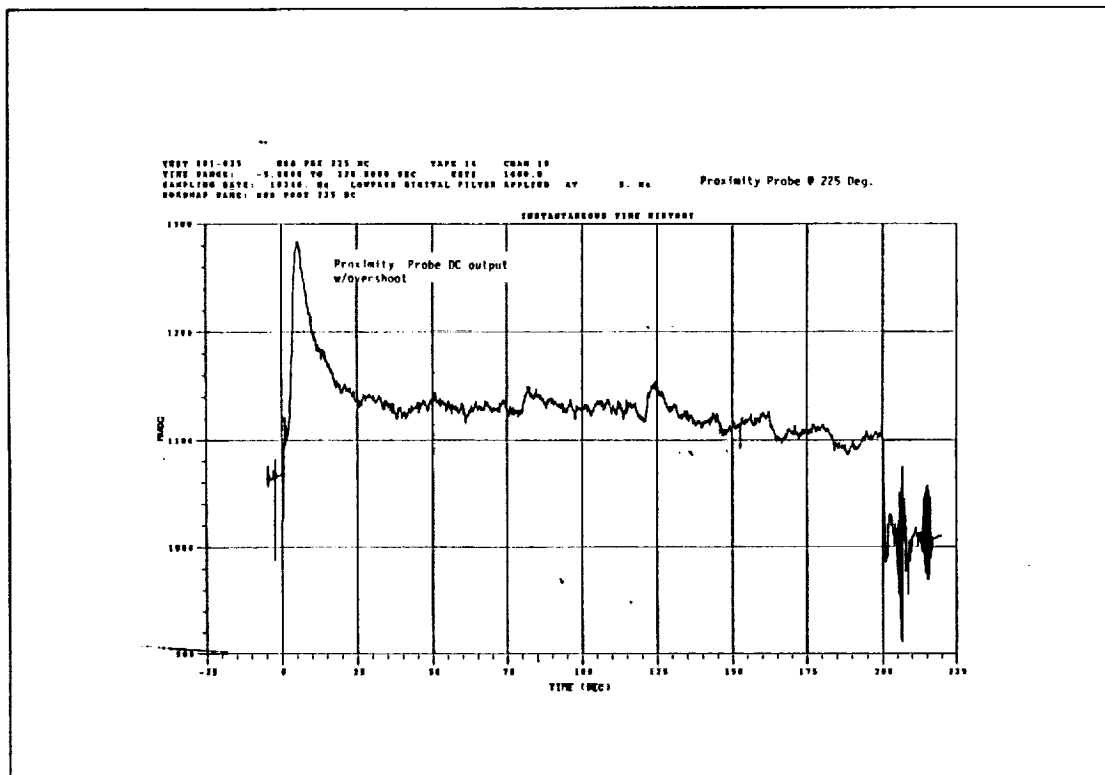


Figure 14. Proximity probe DC output.

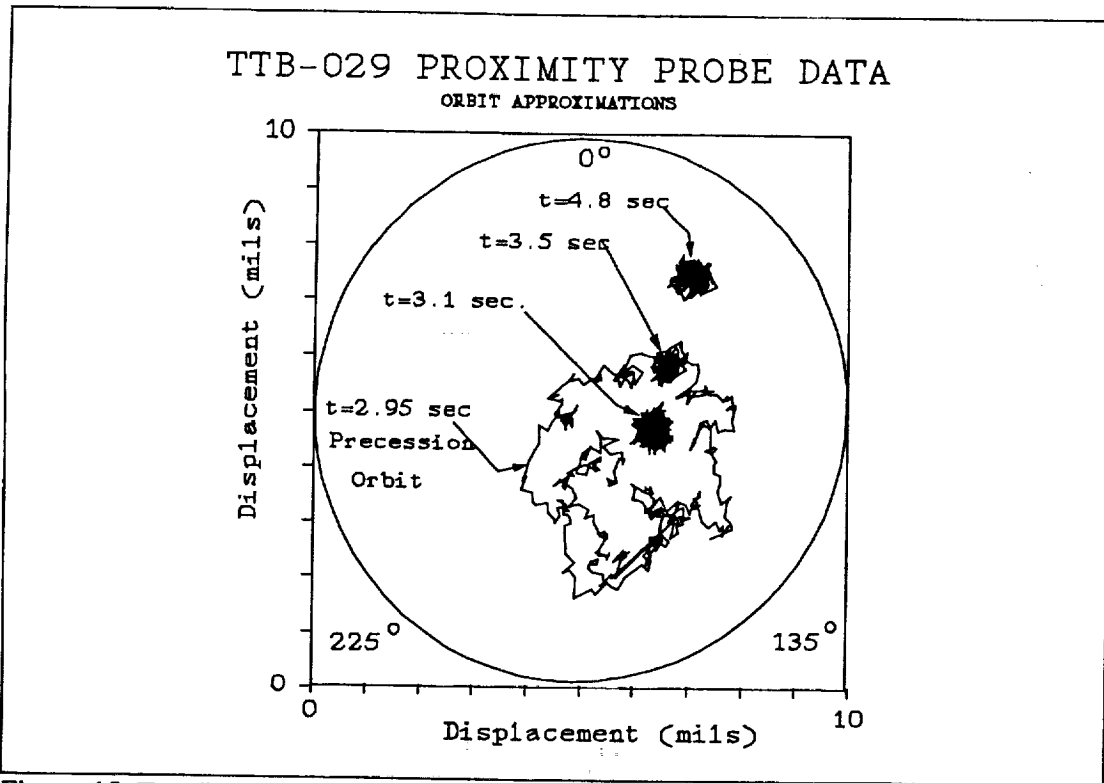


Figure 15. Test #1 Hydrostatic bearing orbit data.

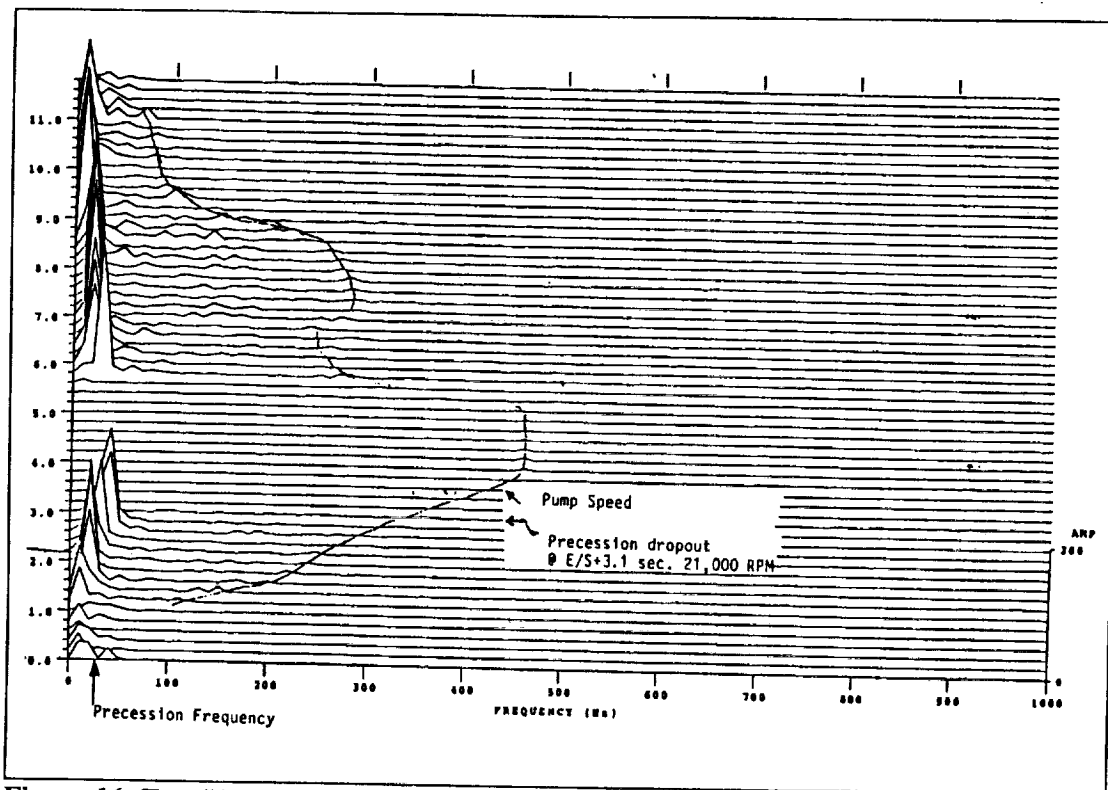


Figure 16. Test #1 proximity probe waterfall data.

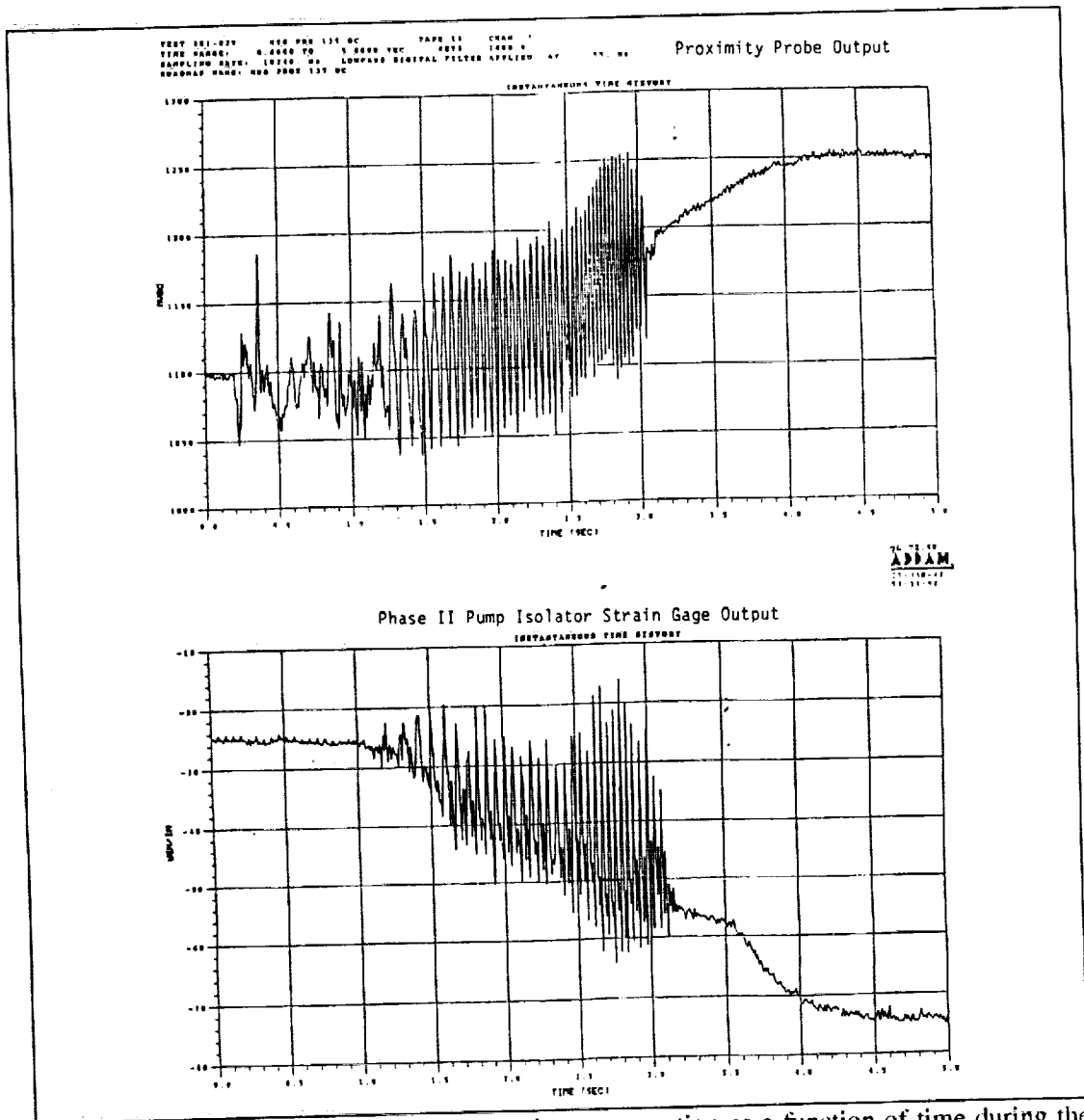


Figure 17. Ball bearing vs. hydrostatic bearing rotor motion as a function of time during the engine start transient.

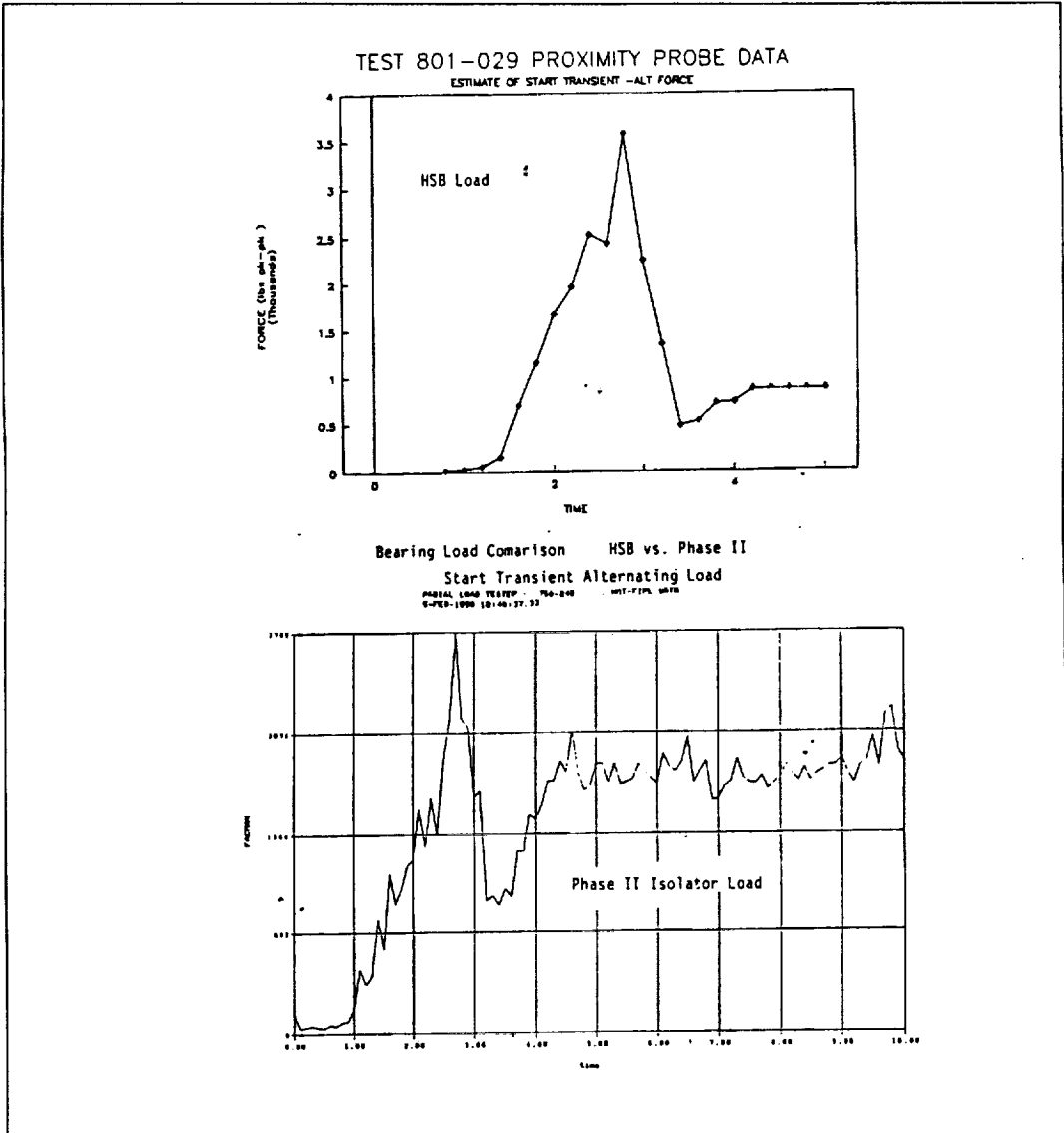


Figure 18. Ball bearing vs. hydrostatic bearing loads as a function of time during the start transient

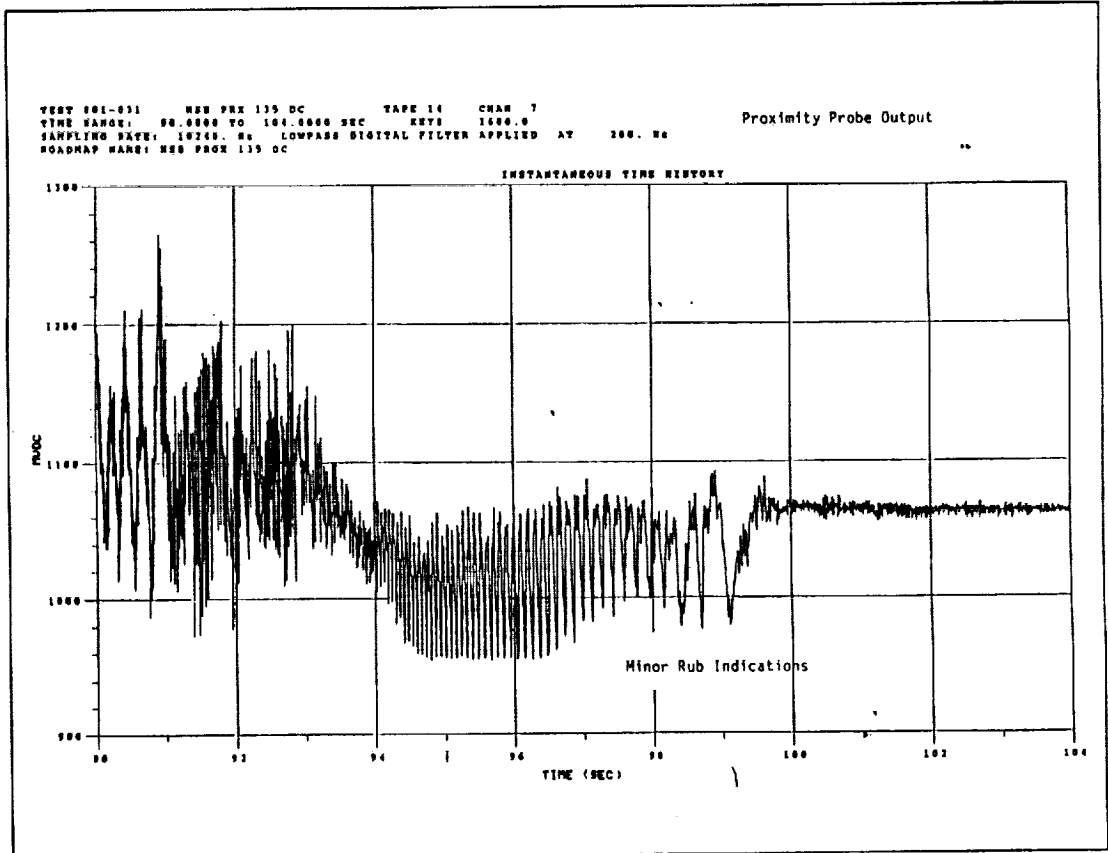


Figure 19. Proximity probe rub indications.

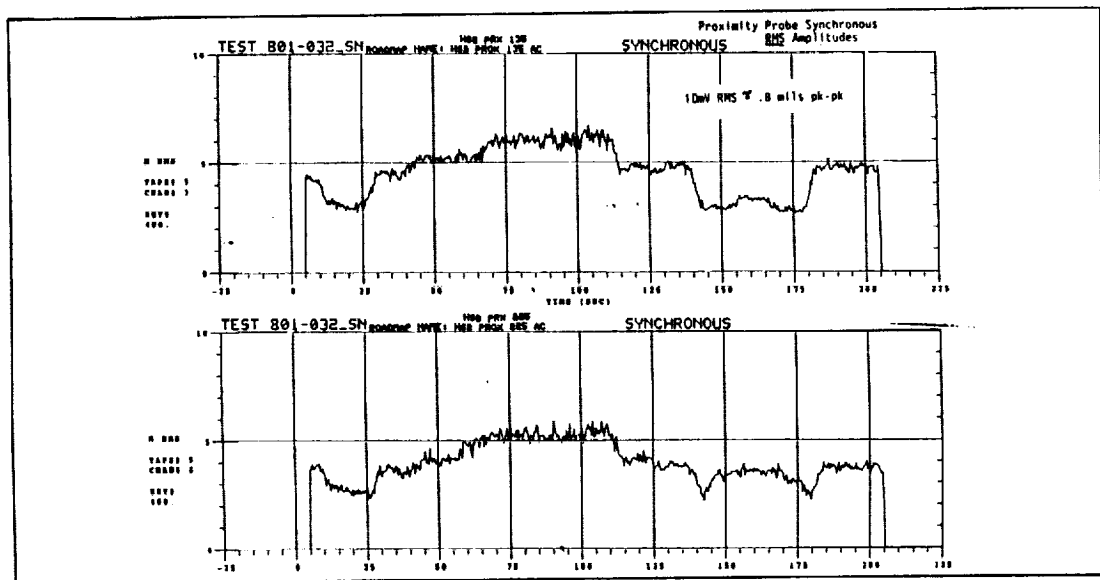


Figure 20. Proximity probe synchronous amplitudes.

TEST TTB-032 PROXIMITY PROBE DATA

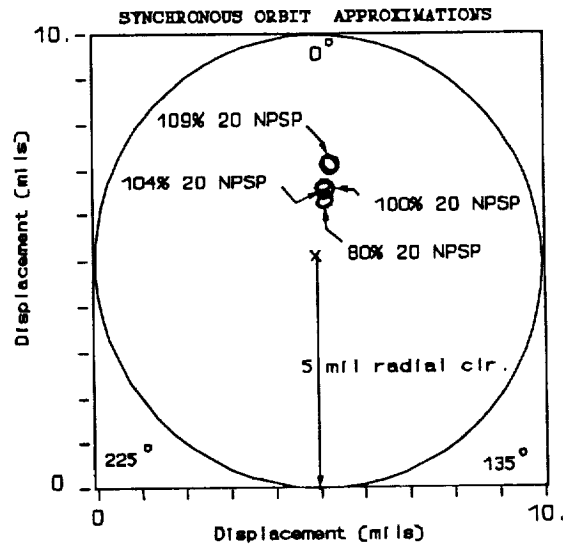


Figure 21. Rotor synchronous orbit amplitudes.

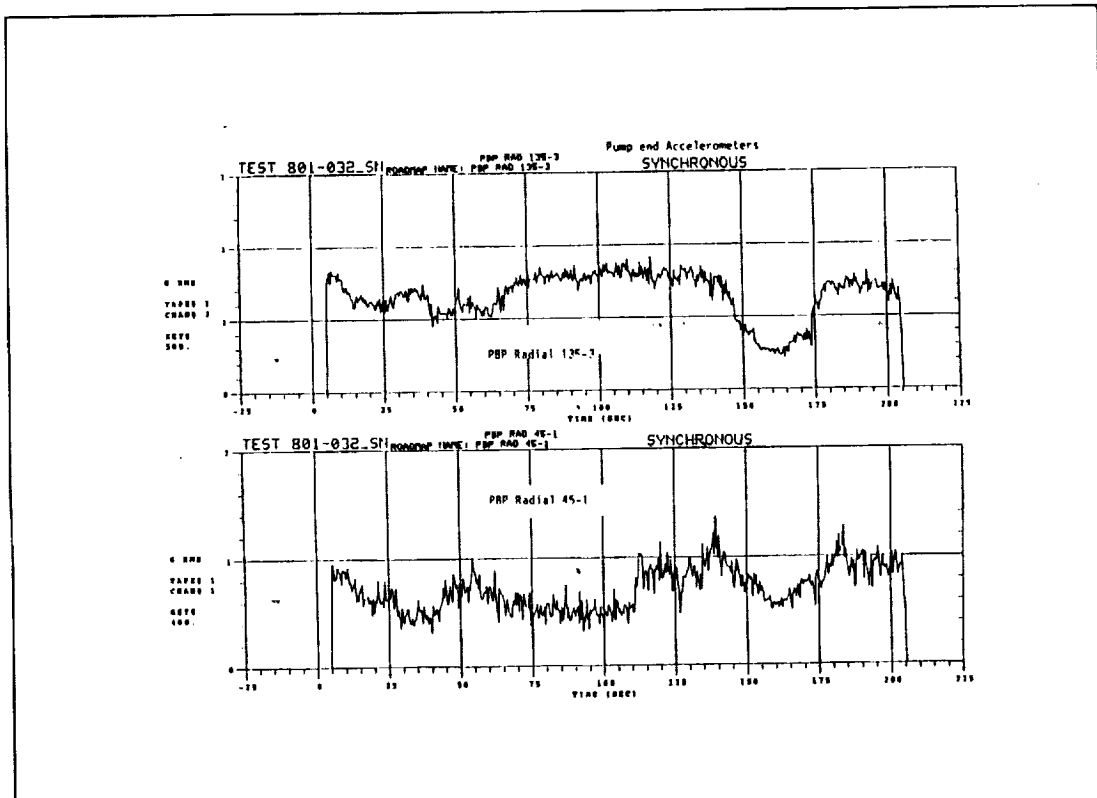


Figure 22. Casing accelerometer synchronous amplitudes.

